Preprints of the 21st IFAC World Congress (Virtual)
Berlin, Germany, July 12-17, 2020

Fabrication and Characterization of a Microfluidic Device with Vertically Aligned Multi Walled Carbon Nanotube Channels

Handan Nak * **Idris Gurkan** * **Hulya Cebeci** * **Ali Fuat Ergenc** *

* *Istanbul Technical University, Istanbul, 34469 Turkey (e-mails: handan.nak@itu.edu.tr, idrisgrkn@gmail.com, geyikh@itu.edu.tr, ali.ergenc@itu.edu.tr)*

Abstract: Microfluidic devices are state of the art technology which are used for many applications especially as lab-on-chips. Manufacturing and characterization of these devices are reported in literature but process control aspects of vertically aligned multiwalled carbon nanotubes are rarely investigated. Furthermore, nano exchange capabilities with such structures are scarcely studied. In this paper, an industrial quality chemical vapor deposition system is designed, built and controlled. A nonlinear PI controller is employed to control the temperature of the chemical synthesis system, where precise temperature control is crucial. This controller behavior depends on the ratio between the error signal and the reference which enables the controller to act faster while avoiding overshoot. A microfluidic nanoexchanger device is manufactured, flow characteristics are modeled and its nanoexchange capability is tested and proven experimentally. These devices have many applications both in industry and biomedical field. One of the promising applications is building artificial organs such as lungs and kidneys where nanoexchanges occur naturally.

Keywords: Carbon nanotubes, microfluidics, chemical vapor depositon, nanoexchange, controlled nano structures.

1. INTRODUCTION

Since their discovery, carbon nanotubes (CNTs) have attracted great interest due to their unique physical, chemical, thermal and mechanical properties. A CNT is simply a nanosized rolled-up graphene sheet that forms a perfect seamless cylinder with fullerene caps at the ends.

Currently, carbon nanotubes are used in a wide variety of disciplines, such as biomedical, pharmaceutical, optics, nanoelectronics and structural reinforcement, due to extremely high mechanical strength with high Young's modulus, having much better electrical and thermal conductivity than copper Smalley (2003); Choi et al. (2004); He et al. (2013); Popov (2004); Purohit et al. (2014). Therefore, the production of high-quality carbon nanotubes with high yield has been the primary goal of many researchers. The chemical vapor deposition (CVD) is the most preferable method for CNT synthesis since it offers an economical and simple production process with high efficiency. In the CVD process, thermal decomposition of a hydrocarbon vapor is achieved in the presence of a metal catalyst in a tube reactor at relatively low temperatures Kumar and Ando (2010). It allows CNT growth in a variety of forms and better control on the growth parameters. Also, CVD is the only solution when it comes to structure and architecture control of CNTs Noy et al. (2007); Kumar and Ando (2010).

⋆ This work was supported by The Scientific and Technological Research Council of Turkey (TUBITAK) with project number 112M807.

CNTs may also be considered as nano-pipes with their nanoscale dimensions, smooth and graphitic walls, showing an extreme compatibility and great environment to transfer and exchange nanomaterials in the fluids. CNTs may have very high aspect ratios which provides them infinite length effect for transfer and exchange with nanometer-scale inner diameter and millimeter-scale heights. In the literature, there are many studies related to the use of CNTs in membranes Xue et al. (2014); Lee et al. (2015); Yoon et al. (2012); Lee and Baik (2010). However, there are not many works that consider nanomaterial exchange along the CNT channels. Material exchange through fluids may be mimicked to design new nanomaterials in a diverse field, similar to biological principles in human body. Air and water molecules may be transported with CNTs as in biological channels. The ultra porosity and permeability of CNTs can have a distinct effect on increasing the efficiency of these nanotube channels.

In this study, vertically aligned multi-walled carbon nanotubes (VA-MWCNT) are synthesized to create small dimension pore sized ultra narrow nanoexchangers for nanoparticle transfer between the channels, utilizing the CVD method. First, an automated chemical vapor deposition system for synthesis is designed and constructed, then high qualified CNTs are synthesized. Temperature control of the chemical synthesis system is a technically challenging procedure to operate due to the high sensitivity of CNTs to the temperature. A nonlinear PI controller with a nonlinear gain connected in series to a constant coefficient linear controller, is employed to control the temperature

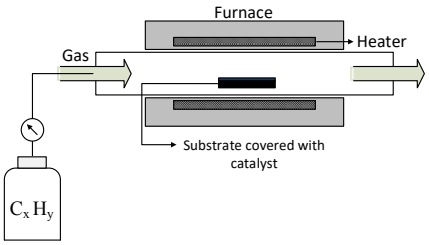

Fig. 1. Schematic diagram of a CVD setup

precisely. Popov stability criterion is employed for the stability analysis of the controller. Then, a novel micro device is designed and fabricated with the VA-MWCNTs. The device provides particle permeability and material exchange through its nanopores. The flow-resistance characteristics of the device are modeled and the nanoparticle exchange behavior is studied within this context.

This paper is organized as follows. The next section presents the CNT synthesis by CVD method. First, the CVD method is introduced with the detailed explanation of the CVD control system. Later, the synthesis process of CNTs is given. In Section 3, fabrication of the micro device is explained. Experimental studies including the pressure characterization and nanoparticle transfer are presented. Finally, in Section 4 the study is reviewed.

2. CNT SYNTHESIS BY CHEMICAL VAPOR DEPOSITION METHOD

2.1 Chemical Vapor Deposition Method

The CVD process involves catalyst-assisted decomposition of hydrocarbons (C_xH_y) in a tubular reactor at 500-900°C. CNTs grow on the catalyst in the reactor, and then are collected when the system cools down to room temperature Popov (2004); Kumar and Ando (2010). Hydrocarbon deposition takes place on the lower peripheral surface of the metal when hydrocarbon vapor contacts with the hot metal nanoparticles, and the dissolved carbon diffuses upward. Thus, the CNTs grow up with the catalyst particle rooted on its base (base-growth model) or they precipitate out across the metal bottom (tip-growth model). Fig. 1 depicts a simple schematic of the experimental set-up used for CVD method.

The key of CNT growth by CVD is to achieve optimal selection of hydrocarbon and catalyst materials, and the precise control of gas flow rate and most importantly control of the pyrolysis temperature. Hydrocarbons such as methane, ethylene, acetylene, xylene, toluene, benzene are generally used as the carbon sources. Catalysts are nanometers of metal particles and are required to activate hydrocarbon decomposition. Best results are obtained with iron, nickel and cobalt nanoparticles as catalyst due to high carbon solubility and diffusion rate Popov (2004). Pyrolysis is defined as the process of thermal conversion of an organic material using a catalyst in the inert atmosphere. Pyrolysis temperature is a key factor affecting diameter of CNTs, mass increasing rate and adsorption efficiency Wang et al. (2012); Kumar and Ando (2010). Even, the thermal gradient that is not controlled properly can cause CNT growth to stop. By controlling the reaction temperature and gas flow rate, CNTs with different

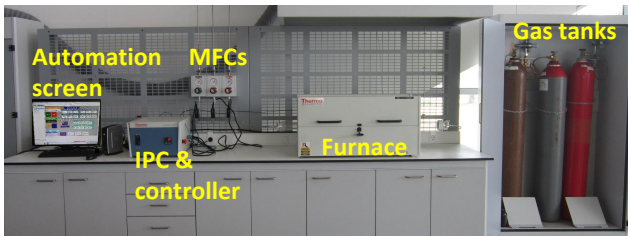

Fig. 2. CVD setup for CNT synthesis

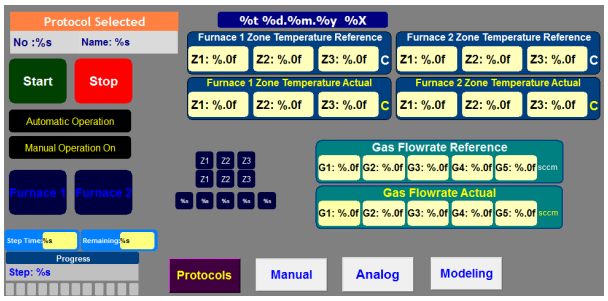

Fig. 3. Automation system main screen

structures may be achieved Li et al. (2002); Kumar and Ando (2005, 2010). In general, low-temperature assists for multi-wall CNTs, while high-temperature yields single-wall CNTs. Therefore, the control of reaction temperature is the highest critical requirement.

2.2 CVD Automation System

As the first step of this study, a carbon nanotube production system using the thermal CVD method with full control and automation is established. The system consists of a tube furnace, a quartz tube with an inner diameter of 25 mm, gas tanks, gas circulation pipes and gas mass flow controllers (MFCs). A photograph of CVD setup for CNT synthesis is given in Fig. 2. Quartz tube is preferred as the reaction chamber due to its resistance to high temperatures and sudden temperature changes, not reacting with gases at these temperatures and transparency. MFCs are utilized for the desired stable gas flow of the process. On board PD type controllers are employed and their proportional and derivative gains are set to 100 and 5000, respectively according to the manufacturer's recommendations. An industrial computer (IPC), which is responsible for the execution of the process stages and precise control of operations, is employed as the controller hardware of the automation system. The automation program is developed by authors to control the temperature of the furnace and set flow rates of the gases as the CNT synthesis protocols dictate (see Fig. 3).

In the industrial furnace (Lindberg/Blue M^{TM} 1200°C Split-Hinge Tube Furnace), the heating element is formed by embedding the sinusoidal-shaped resistance cables into the insulating material. The temperature is measured using a thermocouple at the horizontal center of the furnace. The average voltage applied on the heater resistance of the furnace is controlled via a solid state relay using pulse width modulation (PWM) technique driven by the IPC. The furnace is operated in open loop with constant voltage

input (44 V corresponding to 20% duty cycle) and the temperature is measured to obtain the heating profile of the furnace (see Fig. 4). The model of the system is nonlinear due to nonuniform heat losses depending on temperature differences. Although the model is nonlinear, the heating characteristic of the furnace may be considered as a typical first order thermal system with a certain degree of error margin. The time constant of $2500s$ and the gain of $16^oC/V$ are determined for the first order model that represents the system.

Conventionally, basic PI controllers are employed to control the temperature of these kind of furnaces in practice. However, the precision control of the pyrolysis temperature is crucially critical. The temperature controller should have two important extra features to increase the efficiency and productivity of CNT synthesis. First issue is that there should be no overshoot for temperature of the furnace, which inhibits the growth of the CNT forest. The second one is the thermal gradient which corresponds to designated period of time to reach the target temperature. If the gradient is too steep or too gentle, catalysis may not be properly activated and growth efficiency deteriorates. Thus, the nonlinear PI controller in Ergenc et al. (2017) is utilized to improve the performance of the control action. This controller has error dependent proportional and integral gains which enable the controller to act faster against the disturbances and sudden reference jumps, while preventing overshoot by decreasing of the integral gain exponentially when error is close to zero. Furthermore, the gains nonlinearly increase up to a limited value when the error rises. Structure of the controller is as follows Ergenc et al. (2017):

$$u(t) = \left[k_p e(t) + k_i \int_0^t e(t)dt\right] k(e,r) \tag{1}$$

where, $u(t)$ is the control signal, $e(t)$ is the error signal, $r(t)$ is the reference signal, k_p and k_i are constant gains. The nonlinear gain $k(e,r)$ is a function of $e(t)$ and $r(t)$ as follows:

$$k(e,r) = \gamma - \alpha e^{-\beta\delta} \tag{2}$$

where $\delta = |e(t)/r(t)|$ and, α, β and $\gamma \in \mathbb{R}^+$ are controller design parameters. It is worthy of note that the $k(e,r)$ function is bounded in $[\gamma - \alpha, \gamma]$ with this definition. The main advantage of this structure is the nonlinear gain is not only a function of the error, but also the reference signal which emphasizes the relative ratio of the error to the reference.

The proportional and integral gains of the conventional PI controller part are determined as $k_p = 570$ and $k_i = 0.5$ to achieve 1.05 s of settling time for one degree increment which provides excellent reference temperature tracking. It should be noted that at the full duty cycle of the PWM (full heating power) the maximum temperature gradient is $1.1^oC/s$ in heating mode which is limited with the heating power of the resistances. Here, the nonlinear part of the controller ensures to have high heating capability during the large changes in the reference, while providing a moderate behavior approaching the steady state region which avoids overshoot in the temperature. In addition, this controller delivers fast disturbance rejection with variable gains which are nonlinear function of the error.

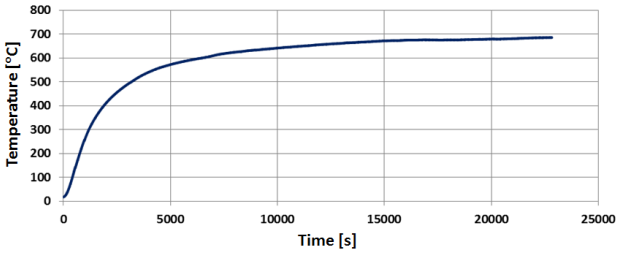

Fig. 4. Open loop response of the furnace for %20 of the full power input

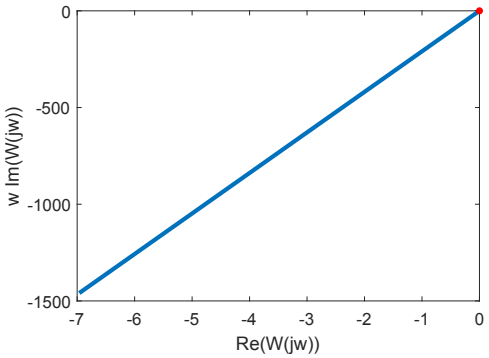

Fig. 5. Popov plot for the stability analysis

The parameters of the nonlinear gain function of the proposed controller are obtained empirically as $\gamma = 2$, $\beta = 0.2$ and $\alpha = 0.8$ after several experimental studies for best performance.

Popov stability criterion is employed for the stability analysis. The Popov criterion states a sufficient condition for the closed loop system to be globally asymptotic stable for all nonlinear gain in the sector $0 \leq k(e,r) \leq k(e,r)_{max}$. This means that the Popov plot of $W(j\omega)$, which is the forward transfer function of the linear part of the system with linear PI controller, must lie entirely on the right of a straight line with a nonnegative slope passing through the point $1/k(e,r)_{max}$ Khalil (2002). The real and imaginary components of $W(j\omega)$ are given below.

$$R_e(W(j\omega)) = \frac{-10880\omega^2}{2500^2+\omega^4+\omega^2} \tag{3}$$

$$\omega I_m(W(j\omega)) = \frac{-22800000\omega^2-8}{2500^2+\omega^4+\omega^2} \tag{4}$$

The Popov plot is obtained as in Fig. 5. It is possible to plot a straight line passing through the origin with nonnegative slope while the Popov plot of $W(\omega)$ entirely lies on the right of this line. Hence, with these parameters the system is globally asymptotic stable. Therefore, $\alpha < \gamma$ is the only condition for the stability of the entire system since $k(e,r)$ function is bounded in $[\gamma - \alpha, \gamma]$. There is no constraint for β parameter for stability (see Ergenc et al. (2017)). As a result, the assignment of $\gamma = 2$, $\beta = 0.2$ and $\alpha = 0.8$ parameters are acceptable for this system.

As an example, the temperature reference profile of a 3-step production protocol in Table 1 is executed. Due to the maximum gradient of the furnace, the temperature reference of the furnace is shaped as depicted in Fig. 6. As seen from the figure, the temperature follows the temperature profile in the capacity of the furnace without

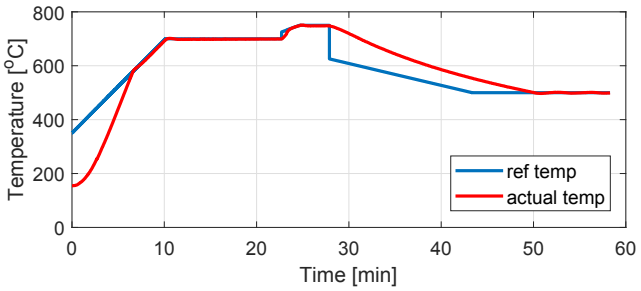

Fig. 6. Temperature control of the furnace

overshoot, and then it is kept constant during the synthesis periods. There is no cooling mechanism, thus the furnace cools down naturally.

Table 1. A sample 3-step production protocol

Step	Duration [min]	Rise time [min]	Temperature [°C]
1	12	10	700
2	3	2	750
3	8	15	500

2.3 Synthesis of CNTs

Vertically-aligned (VA) MWCNTs are synthesized by the thermal CVD to be used in microfluid device. Single-crystal silicon (Si) wafer is used as the substrate. Catalyst layers are deposited on oxidized (300 nm thick) silicon wafer by an electron beam evaporator (chamber pressure 2.610^{-6} Torr). Aluminum oxide (Al_2O_3) is deposited as a buffer layer (10 nm thick) followed by a 3 nm thick iron (Fe) catalyst layer.

Helium (He) and hydrogen (H_2) gases are used as the carrier gas and ethylene (C_2H_4) is used as carbon source. The synthesis protocol in Table 2 is executed by automatic CVD system described in the previous section. Synthesis of VA-MWCNTs starts by nucleation of an end-cap fragment on the catalyst particles and followed by vertically nanotube growth through accumulation of carbon atoms on the surface of the substrate.

Table 2. Production protocol for MWCNT

Step	He [sccm]	H_2 [sccm]	C_2H_4 [sccm]	Duration [min]	Temp. [°C]
Nucleation	1600	1000	0	15	750
Growth	1000	500	300	15	750

The height, volume fraction and orientation of synthesized VA-MWCNTs are determined via scanning electron microscope (SEM). The SEM images are given in Fig. 7 and Fig. 8. CNTs are vertically aligned and have a volume fraction of 1%. They are approximately 1.5 mm high. This height is quite impressive considering that production is performed by thermal CVD under atmospheric conditions without the assistance of water.

3. FABRICATION AND CHARACTERIZATION OF MICROFLUIDIC DEVICE WITH VA-MWCNTS

3.1 Fabrication of the Device

In this study, a 3-channel micro device consisting of two rows of CNTs is produced. CNT walls have nano-level

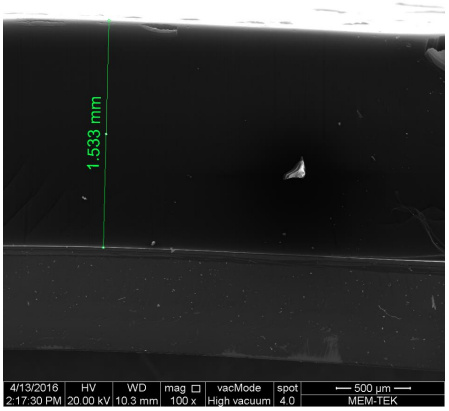

Fig. 7. SEM image of synthesized vertical aligned MWCNTs (VA-MWCNT) at a magnification of $100x$

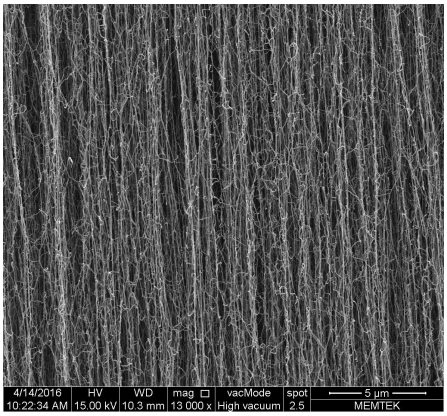

Fig. 8. SEM image of synthesized vertical aligned MWCNTs (VA-MWCNT) at a magnification of $13000x$

porous ($< 50nm$) structures, thus only molecules and nanoparticles may pass through these walls. CNT walls are produced with slope to increase the interaction between CNT walls and nanoparticles for high permeability.

Photolithography is used for the production of patterns on the silicon wafer. It is the process of transferring geometric shapes on a mask to the surface of the silicon wafer. The process is applied to the catalyst covered wafer. At the end, non photo-resist regions remain catalyst covered and CNTs grow only on these regions. The device is isolated with a polymer in order to study the behavior under flow after patterned CNT growth. The enclosure for the microchannels are built using polydimethylsiloxane (PDMS) elastomer which is molded in a template. The surface of silicon wafer is processed by laser to adhere the PDMS onto the smooth, glossy silicon wafer. Then, VA-MWCNTs are synthesized by CVD automation system as explained earlier. Optical microscope images of the device without PMDS cover is given in Fig. 9. Finally, the microchannels is covered with PMDS enclosure and the input and output openings are formed by via branules (see Fig. 10).

3.2 Characterization of the Device

In microfluidics and lab-on-a-chip systems, control of fluid motion is essential in almost all applications. In microsys-

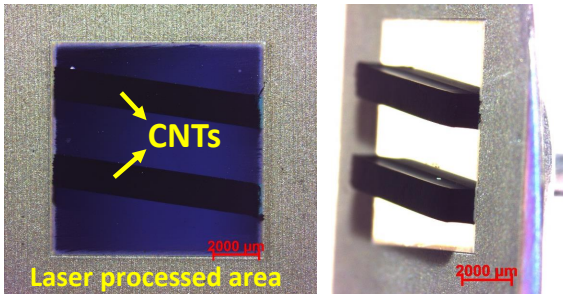

Fig. 9. Optical microscope images of the patterned carbon nanotube

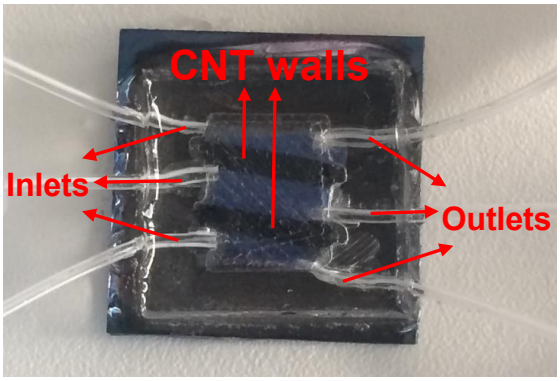

Fig. 10. Picture of microfluid device with input and output channels

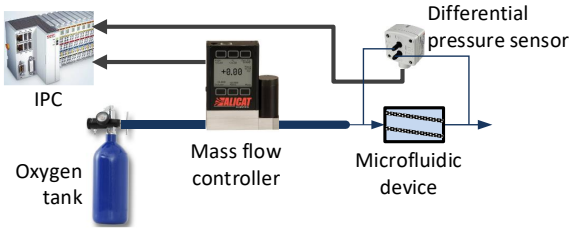

Fig. 11. Test system for pressure drop under oxygen flow

tems, fluid flow is monitored through pressure drop measurements; and reversibly, fluid flow may also be driven by pressure control Chung et al. (2009). Pressure drop in a microchannel for laminar flow is expressed as

$$\Delta P = QR \tag{5}$$

where ΔP is the difference in pressure, and Q is the volumetric rate of flow of liquid between two points in a channel. These two terms are proportional; the constant of proportionality is called the fluidic resistance, R Fuerstman et al. (2007); Cheung et al. (2012).

Device characteristic under one phase (gas) flow Oxygen gas at increasing flow rates is passed through the device's middle channel and the pressure drop in the device is measured by a differential pressure sensor located between the inlet and outlet of the channel. The schematic of the test system are given in Fig. 11. Fig. 12 exhibits a simplified block diagram of the open-loop system used to model the device.

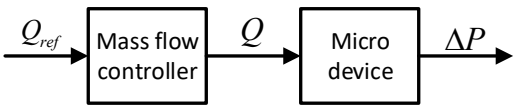

Fig. 12. Open loop block diagram of the test system

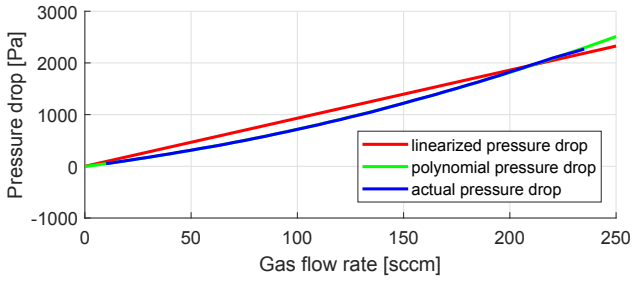

Fig. 13. Pressure drop against one phase flow rate

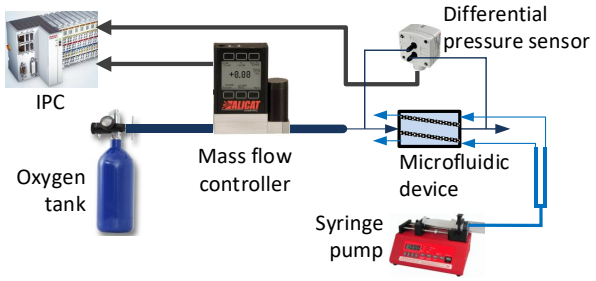

Fig. 14. Test system for pressure drop under two phase flow

The relationship between oxygen flow rate and pressure drop is given in Fig. 13. The change in pressure difference is expressed with second order polynomial as follows.

$$\Delta P = 0.0191Q^2 + 5.2745Q - 1.5547 \tag{6}$$

The first order form is expressed as

$$\Delta P = 9.8424Q - 186.1321. \tag{7}$$

The slope of that line gives the device's fluidic resistance and it is found as $R = 9.8424\ Pa/sccm$.

Device characteristic under two-phase (gas-liquid) flow For this characteristic, oxygen gas passes through the middle channel of the device while water flows across the two side channels in the opposite direction. A controlled syringe pump is utilized to create the water flow. In the micro device, the pressure of both phase flows has to be close to each other to prevent damage on the channel walls due to the pressure difference. It is also important not to force one fluid to pass to other channel creating either bubbles in water or flooding of gas channel. Isopressure flows also increase the efficiency of nanoparticle exchange by diffusion. The test system is presented in Fig. 14. The gas flow pressure drop curve is depicted in Fig. 15. The water flow rate is increased via the syringe pump in direct proportion to the gas flow rate during the operational test.

The second order and first order models of the device are obtained as in (8) and (9). The device resistance is determined as $R = 12.0873\ Pa/sccm$. Flow resistance is higher in the middle channel as expected when the water passing through the two of the three channels.

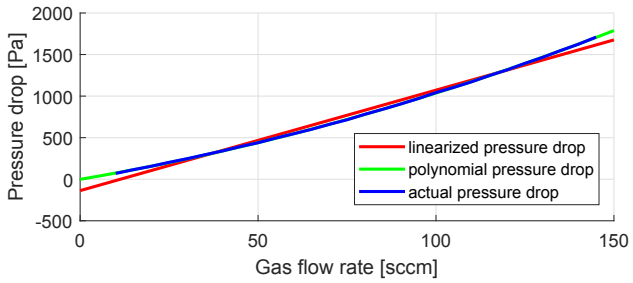

Fig. 15. Pressure drop against two-phase flow rate

$$\Delta P = 0.031Q^2 + 7.2778Q - 1.264 \quad (8)$$

$$\Delta P = 12.0873Q - 137.0159 \quad (9)$$

Gas molecules are diffused into the water in nano-level (without creating bubbles) during the two phase flow as desired. Dissolved oxygen level in the water is measured when entering and exiting the micro device to observe this nanoparticle exchange. The amount of dissolved oxygen is measured before and after the flow as 8.31 ppm (104.2%) and 9.54 ppm (119.6%), respectively. The measurements presents a 15% increase in the oxygen concentration. Thus, it is shown that the concept of carbon nanotube walled nanoparticle exchange system works.

4. CONCLUSION

In summary, a novel 3-channel microfluidic device with VA-MWCNT walls on a silicon wafer with a PDMS enclosure is designed and manufactured. The synthesis of high quality nanotubes is achieved easily and successfully utilizing a state of the art control and automation system for the CVD. The micro device separates the cross-flows with a nano-porous VA-MWCNT membrane and particles are exchanged through this membrane. It is known that CNT has many applications in industry and this paper reports one as nanoparticle exchanger. These nano exchangers may be utilized as artificial organs such as lungs and kidneys where nano exhanges occur between gas-liquid and liquid-liquid phases naturally. Furthermore, a simple and useful characterization and testing method is presented which may also help to explain the transport mechanism of fluids in the nanochannels compared to existing models.

REFERENCES

Cheung, P., Toda-Peters, K., and Shen, A.Q. (2012). In situ pressure measurement within deformable rectangular polydimethylsiloxane microfluidic devices. *Biomicrofluidics*, 6(2), 026501.

Choi, W.B., Bae, E., Kang, D., Chae, S., Cheong, B.h., Ko, J.h., Lee, E., and Park, W. (2004). Aligned carbon nanotubes for nanoelectronics. *Nanotechnology*, 15(10), S512.

Chung, K., Lee, H., and Lu, H. (2009). Multiplex pressure measurement in microsystems using volume displacement of particle suspensions. *Lab on a Chip*, 9(23), 3345–3353.

Ergenc, A.F., Nak, H., and Akkaya, Ş. (2017). Design, analysis and experimental verification of a novel nonlinear pi controller. *Anadolu University Journal of Science and Technology A - Applied Sciences and Engineering*, 18(4), 876–896.

Fuerstman, M.J., Lai, A., Thurlow, M.E., Shevkoplyas, S.S., Stone, H.A., and Whitesides, G.M. (2007). The pressure drop along rectangular microchannels containing bubbles. *Lab on a Chip*, 7(11), 1479–1489.

He, H., Pham-Huy, L.A., Dramou, P., Xiao, D., Zuo, P., and Pham-Huy, C. (2013). Carbon nanotubes: applications in pharmacy and medicine. *BioMed research international*, 2013.

Khalil, H. (2002). *Nonlinear Systems*. Pearson Education. Prentice Hall.

Kumar, M. and Ando, Y. (2005). Controlling the diameter distribution of carbon nanotubes grown from camphor on a zeolite support. *Carbon*, 43(3), 533–540.

Kumar, M. and Ando, Y. (2010). Chemical vapor deposition of carbon nanotubes: a review on growth mechanism and mass production. *Journal of nanoscience and nanotechnology*, 10(6), 3739–3758.

Lee, B., Baek, Y., Lee, M., Jeong, D.H., Lee, H.H., Yoon, J., and Kim, Y.H. (2015). A carbon nanotube wall membrane for water treatment. *Nature communications*, 6, 7109.

Lee, C. and Baik, S. (2010). Vertically-aligned carbon nano-tube membrane filters with superhydrophobicity and superoleophilicity. *Carbon*, 48(8), 2192–2197.

Li, W., Wen, J., and Ren, Z. (2002). Effect of temperature on growth and structure of carbon nanotubes by chemical vapor deposition. *Applied Physics A*, 74(3), 397–402.

Noy, A., Park, H.G., Fornasiero, F., Holt, J.K., Grigoropoulos, C.P., and Bakajin, O. (2007). Nanofluidics in carbon nanotubes. *Nano today*, 2(6), 22–29.

Popov, V.N. (2004). Carbon nanotubes: properties and application. *Materials Science and Engineering: R: Reports*, 43(3), 61–102.

Purohit, R., Purohit, K., Rana, S., Rana, R., and Patel, V. (2014). Carbon nanotubes and their growth methods. *Procedia materials science*, 6, 716–728.

Smalley, R.E. (2003). *Carbon nanotubes: synthesis, structure, properties, and applications*, volume 80. Springer Science & Business Media.

Wang, L.p., Huang, Z.c., Zhang, M.y., and Liao, X.s. (2012). Effect of pyrolysis temperature on properties of acf/cnt composites. *Journal of Central South University*, 19(10), 2746–2750.

Xue, C., Du, G.Q., Chen, L.J., Ren, J.G., Sun, J.X., Bai, F.W., and Yang, S.T. (2014). A carbon nanotube filled polydimethylsiloxane hybrid membrane for enhanced butanol recovery. *Scientific reports*, 4, 5925.

Yoon, D., Lee, C., Yun, J., Jeon, W., Cha, B.J., and Baik, S. (2012). Enhanced condensation, agglomeration, and rejection of water vapor by superhydrophobic aligned multiwalled carbon nanotube membranes. *ACS nano*, 6(7), 5980–5987.